THE ASTROPHYSICAL JOURNAL, 426:604–611, 1994 May 10

SPECTRAL EVOLUTION OF A SUBCLASS OF GAMMA-RAY BURSTS OBSERVED BY BATSE

P. N. BHAT,[1,2] GERALD J. FISHMAN, CHARLES A. MEEGAN, ROBERT B. WILSON, CHRYSSA KOUVELIOTOU,[3]
WILLIAM S. PACIESAS,[4] AND GEOFFREY N. PENDLETON[4]
ES-66 Space Science Laboratory, NASA/Marshall Space Flight Center, Huntsville, AL 35812

AND

BRADLEY E. SCHAEFER[3]
NASA/Goddard Space Flight Center, Code 661, Greenbelt, MD 20771
Received 1993 September 3; accepted 1993 November 11

ABSTRACT

Among the gamma-ray bursts observed by the Burst and Transient Source Experiment (BATSE) on board the *Compton Gamma Ray Observatory* we define a subclass of bursts based on similar morphology: a sharp rise followed by a longer decay time. About 7% of all the gamma-ray bursts observed by BATSE fall into this subclass. We study the spectral evolution of these bursts by fitting models to time-segmented burst spectra and find no clear distinction between the spectral evolutionary properties of this subclass and those of other bursts. Further, we study the high time resolution spectral evolution of this subclass of GRBs using their spectral hardness ratios. A majority of the bursts show hardness ratio leading the counting rate and also display a continuous hard to soft evolution. The time lag between the counting rate and the hardness ratio is found to be directly correlated with the rise time of the counting rate profile. We also find, for the first time, evidence for spectral variation in a timescale of 64 ms.

Subject heading: gamma rays: bursts

1. INTRODUCTION

One of the characteristics of a "classical" gamma-ray burst (GRB) is its hard energy spectrum, often with a very high energy tail extending up to hundreds of MeV (Cline et al. 1973; Cline & Desai 1975; Matz et al. 1985; Schneid et al. 1992). These spectra are remarkable in that nearly all of the emission is at γ-ray energies: the power per logarithmic energy interval rises steeply in all burst spectra at low energies and generally peaks above 100 keV.

Spectral variability is a general feature of GRBs (Mazets et al. 1982). GRB spectra seem to be variable on timescales as short as the detector time resolution, and there is some indication of a correlation between temporal variability of luminosity (derived from the count spectra) and parameters measuring the hardness, such as the temperature (Mazets et al. 1982; Golenetskii et al. 1983). Generally, luminosity increases with spectral hardness, but the spectra of different GRBs do not always show an unambiguous correlation of luminosity with temperature (Kargatis et al. 1991; Bhat et al. 1992a).

A hard-to-soft spectral evolution in the 50 keV–2 MeV energy range has also been observed in many GRBs with durations greater than 1 s (Norris et al. 1986). However, there are several exceptions to this general behavior. Jourdain (1990) analyzed the count spectra of several bursts observed by the APEX experiment and concluded that spectral evolution has no correlation with the time history. In short, GRB spectra display diverse spectral evolution properties (Band et al. 1993).

In this paper we study the spectral evolution characteristics of a subclass of GRBs identified by similar morphology. We have selected a sample of bursts which have a short rise time (≤ 4.0 s) and a nearly exponential decay. Events with this distinct morphological feature were identified in an earlier study by Kouveliotou et al. (1991) as comprising a subclass. Kouveliotou et al. show that the average peak hardness ratio of a sample of eight such GRBs is significantly higher compared to that for bursts with more symmetric profiles. Our set of 19 bursts (Table 1) includes the previous subset of events. Some of the GRBs chosen have a smooth profile, while others are highly structured. The latter are included because the envelope of the subpulses during the decay phase has an almost exponential shape. Our analysis utilizes the Large Area Detector (LAD) data which provide good statistics for weaker bursts. The question we address here is whether the bursts in this subset with similar time profiles and possibly higher average peak hardness ratio, exhibit spectral evolution properties in common which differ from those of other GRBs.

2. OBSERVATIONS AND DATA SYSTEM

The Burst and Transient Source Experiment (BATSE) on board the *Compton Gamma Ray Observatory* (CGRO) consists of eight identical detector modules. Each module includes a large area NaI(Tl) detector (LAD) and a smaller spectroscopy detector (SD) with higher energy resolution. The faces of the LADs are parallel to the surfaces of a regular octahedron, thus providing a complete visibility of the sky not occulted by Earth. A LAD consists of a NaI(Tl) crystal 20 inches (50.8 cm) in diameter and 0.5 inches (1.3 cm) thick with an energy resolution of $\sim 27\%$ at 88 keV. The energy range is from 25 to 2000 keV. The energy resolution of the 128 channel LAD spectra is 5 keV per channel below 300 keV, 10 keV per channel in the range 300–600 keV, and 40 keV per channel above 600 keV. The present analysis utilizes the high-energy resolution spectral data types (HER and HERB) and the low-energy resolution data types (PREB and DISCSC) (Fishman et al. 1989).

[1] NRC/NAS Senior Resident Research Associate.
[2] On leave from Tata Institute of Fundamental Research, Bombay 400 005, India.
[3] University Space Research Association.
[4] Department of Physics, University of Alabama in Huntsville, AL 35899.

TABLE 1

SUMMARY OF TEMPORAL CHARACTERISTICS OF BURSTS IN THE SELECTED SAMPLE

Burst Name	Time Lag (s)	Rise Time (s)	Total Counts	Duration (T_{90}, s)[a]	Mean HR	Maximum HR
1B 910421	...	0.576	80036	5.184	0.37 ± 0.02	0.45 ± 0.02
1B 910602	...	0.448	95059	80.832	0.77 ± 0.01	1.5 ± 0.2
1B 910604	0.128 ± 0.032	0.512	8042	2.944	0.34 ± 0.03	0.98 ± 0.22
1B 910627	0.78 ± 0.032	0.832	122091	15.168	0.43 ± 0.005	0.91 ± 0.09
1B 910629	−0.256 ± 0.064	0.32	40759	37.696	1.0 ± 0.02	1.4 ± 0.01
1B 910714	−0.448 ± 0.064	0.128	8499	4.288	0.99 ± 0.08	3.68 ± 0.91
1B 910717	0.448 ± 0.032	0.256	82311	4.864	0.55 ± 0.006	1.55 ± 0.11
1B 910718B	0.64 ± 0.064	0.704	85652	36.224	0.8 ± 0.01	1.95 ± 0.39
1B 910721	0.512 ± 0.064	1.856	53182	22.528	0.47 ± 0.01	1.34 ± 0.18
1B 910809	0.64 ± 0.16	0.704	44310	20.16	0.72 ± 0.02	1.4 ± 0.24
1B 910814	0.576 ± 0.032	0.832	352166	53.888	1.33 ± 0.01	2.9 ± 0.17
1B 910927	3.584 ± 0.064	3.328	125677	17.344	0.39 ± 0.004	1.4 ± 0.28
1B 911016	0.64 ± 0.064	1.472	72031	13.44	0.55 ± 0.01	1.73 ± 0.09
1B 911022	0.64 ± 0.064	0.768	17283	6.656	0.33 ± 0.02	0.67 ± 0.15
1B 911031	2.084 ± 0.064	3.008	303204	89.984	0.61 ± 0.005	0.95 ± 0.13
1B 911104	0.192 ± 0.032	0.256	43358	6.656	0.8 ± 0.016	1.76 ± 0.14
1B 911118	1.792 ± 0.032	1.792	743529	19.2	0.57 ± 0.002	2.52 ± 0.38
1B 920216	2.88 ± 0.16	3.328	76298	19.968	0.46 ± 0.009	1.07 ± 0.16
2B 921207	0.384 ± 0.032	1.152	539792	10.752	0.55 ± 0.002	1.7 ± 0.045

[a] T_{90} is defined as the duration between the 5% and 95% intensity points on the integral time profile of the burst (Kouveliotou et al. 1993).

The background spectra (high-energy resolution, HER) are stored between triggers, and their accumulation time varies between 16 and 500 s. A burst is detected when the counting rates (in the energy range 50–300 keV) in two or more detectors exceeds 5.5 standard deviations simultaneously. This increase could occur in any of the three trigger times, viz. 64, 256, or 1024 ms. When a GRB is detected, high energy resolution burst (HERB) data accumulation for four LADs begins: the accumulation time depends on the burst intensity and varies in units of 64 ms. The accumulation time is the lowest for spectra from the most illuminated detector, while it is twice as long for the second brightest and four times as long for the third and fourth brightest detectors.

Preburst (PREB) data, which are available for individual detectors, starts 2.048 s before the trigger and the discriminator science data (DISCSC), which is summed over the triggered detectors, lasts for 4 minutes after the trigger. Both PREB and DISCSC data have the same time resolution of 64 ms and have four-channel spectral information with energy band-widths 25–50 keV, 50–100 keV, 100–300 keV, and >300 keV, for channels 1–4, respectively. The low-level discriminator threshold for the LADs is 25 keV. PREB and DISCSC data types were used for deriving the burst hardness ratios as discussed below. A more detailed description of the BATSE data types may be found in Fishman et al. (1989).

3. ANALYSIS

Figure 1 shows a sample of four light curves with a time resolution of 0.064 s, integrated over the complete energy range of the LADs. One can see a variety of shapes and structures in the time histories. Some contain multiple pulses, each with short rise time and long decay times (Fig. 1*c*). Some others show extensive structure within the burst envelope (Fig. 1*b*).

3.1. *Spectral Fitting Technique*

The spectra were analyzed using the BATSE Spectral Analysis Software (BSAS) package (Schaefer et al. 1992). Each burst was subdivided into several segments. The integration time for each segment is chosen so that the background-subtracted spectrum generated for each segment had a statistically significant number of counts, especially at the high-energy end of the spectrum. Consequently the time resolution of the spectra depends on the burst intensity.

A background spectrum for each burst was generated as a polynomial fit to each energy channel of the spectra before and after the burst. The interpolated background spectrum at the trigger time was used to derive the burst spectra for all segments.

The detector response to gamma-ray photons from the burst at different angles to the burst direction is a function of photon energy. A detailed model of the BATSE module and a simplified spacecraft description (Pendleton et al. 1989) have been used to calculate the scattering in the detector environment. Generally, the third and fourth brightest detectors are likely to face Earth and hence detect a significant fraction of photons scattered off Earth's atmosphere in addition to the burst photons. More brightly illuminated detectors are relatively free from this effect. Hence, we used only the spectral data from the brightest or, in some cases, the first two brightest detectors. No correction for atmospheric scattering was used in the detector response model.

The LAD spectra, with a higher statistical accuracy than the SDs, are better suited for the continuum spectral evolution studies. In the present analysis, the spectrum for each segment of the burst was fitted to standard functions either singly or in combination using the canonical forward-folding deconvolution method (Loredo & Epstein 1989). Several functions were tried and the best-fit functions, identified by the lowest χ^2, were finally used for all the spectra in a burst. The function finally chosen for a burst does not necessarily represent the physical process responsible for emission of burst photons at the source, serving instead to parameterize the spectral shape.

The models used, singly or in combination, are as follows:

The power-law (PWER) model:

$$F(E)dE = A\left(\frac{E}{100}\right)^{\alpha} dE\,; \qquad (1)$$

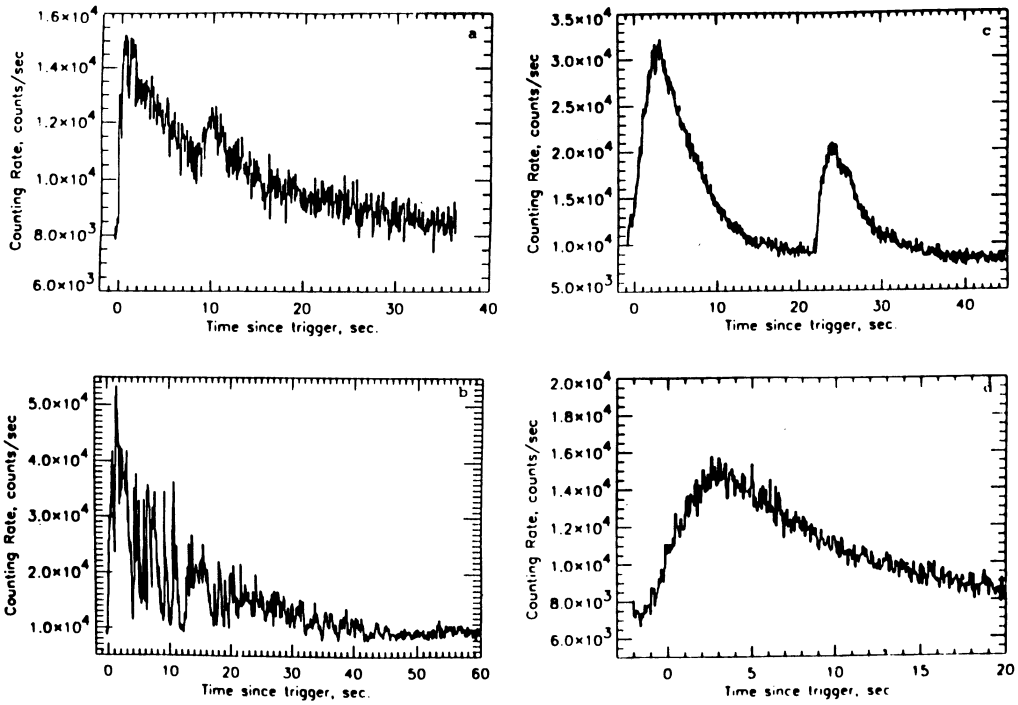

FIG. 1.—Time histories of four typical gamma-ray bursts which belong to the subclass. Burst catalog names whose time profiles which appear here with a time resolution of 64 ms are (*a*) 1B 910602, (*b*) 1B 910814, (*c*) 1B 911031, and (*d*) 1B 920216.

The optically thin thermal bremsstrahlung (OTTB) model:

$$F(E)dE = \left(\frac{A}{T^{1/2}E}\right)e^{-(E/T)}\,dE\,; \qquad (2)$$

The blackbody (BLBD) model:

$$F(E)dE = Ae^{-[(E/T)-1]}\left(\frac{E}{(T)^2}\right)^2 dE\,; \qquad (3)$$

and

The Comptonized spectral (COMP) model:

$$F(E)dE = A\left(\frac{E}{100}\right)^{\alpha}e^{-(E/T)}\,dE\,, \qquad (4)$$

where the model parameters are as follows: A, the normalization constant; T, the temperature in keV; and α, the power-law index; while E is the photon energy in keV. The parameters which represent the spectral hardness are the temperature T (keV) (does not necessarily represent the physical temperature at the source) and the power-law index α. We call α and T as the fitted hardness parameters (FHP).

Figure 2 shows a typical model fit for a spectrum of 1B 910814 from 0.8 to 1.4 s after the trigger. The model represented by the solid line consists of a sum of a blackbody and power-law functions fitted in the energy range 100–1950 keV. The data are shown in count space along with the statistical errors. The χ^2 value of the fit is 117 for 99 degrees of freedom.

Table 2 summarizes the bursts analyzed using BSAS. One can see from the table that in some cases more than one type of model functions was fitted in order to test whether the spectral evolution property is model independent. Also shown in the table are the range of integration times of the segmented spectra (the fifth column) and the energy range used in the analysis (the sixth column).

3.2. *Analysis Using Hardness Ratio*

In order to study the spectral evolution on fine time scales, we also used the four-channel data types which have 64 ms resolution throughout each burst. The background data after

TABLE 2

SUMMARY OF THE SPECTRAL FUNCTIONS USED DURING THE BURST ANALYSIS WITH BSAS

Burst Name	Model	Number of Parameters	Number of Spectra	Range of Integration Times (s)	Energy Range (keV)
1B 910602	OTTB	2	9	0.896–7.42	100–1950
1B 910629	OTTB	2	6	0.384–6.33	100–1500
1B 910717	OTTB	2	7	0.64 –1.34	100–1500
1B 910718B	COMP	2	8	0.832–4.42	50–1950
1B 910814	COMP	2	16	0.768–2.56	50–1900
	BLBD + PWER	4			40–1900
1B 920216	OTTB	2	14	0.832–4.352	50–1950
	PWER	2	14		
2B 921207	COMP	2	16	0.192–3.072	50–1950

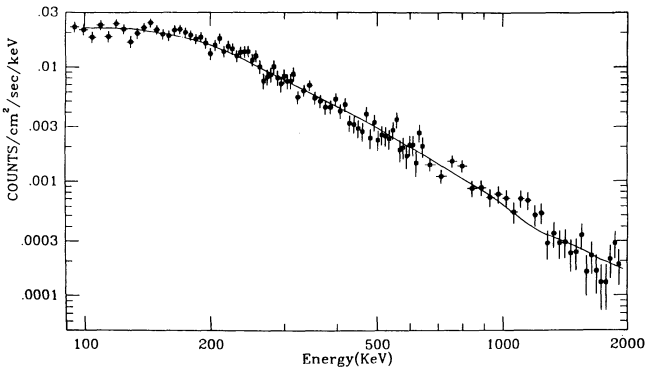

FIG. 2.—A typical spectrum from 1B 910814 during 0.8–1.4 s after the burst trigger, fitted to a spectral model shown in eq. (4) (see text). The solid line is the model, while data points are shown in count space along with the statistical errors. The model does not seem to fit the data at the low and high ends of the energy bandwidth.

the burst were fitted to a polynomial and subtracted from the counting rates during the burst for each of the four energy channels. We define spectral hardness ratio as the ratio of that net count rate above 100 keV to that in the range 25–100 keV.

Systematic errors which effect the use of hardness ratios for spectral analysis have been discussed by Schaefer (1993). In particular, Schaefer noted the potential correlation between the hardness ratio and burst count rate. To investigate this effect, we also computed a hardness ratio using only those channels which the instrument employs for burst detection: 50–100 keV and 100–300 keV. A comparison of spectral evolution using both hardness ratios for a subset of bursts showed no significant difference. We used our initial definition of the hardness ratio for further analysis.

4. RESULTS

4.1. *Results from the Spectral Fitting Analysis*

Figure 3 shows the variation of the spectral hardness parameter ("temperature") as a function of burst intensity for four typical events. While a small number of bursts (two of a total of 19 bursts in this subclass) show no significant spectral evolution during the entire burst (Fig. 3*a*), most exhibit varying degrees of positive correlation of spectral hardness with burst intensity (Figs. 3*b* and 3*c*). In Figure 3*c* the fitted model consists of a sum of a blackbody function and a power-law function. Since the power law can fit a hard tail as shown in Figure 2, it is possible, in principle, that the blackbody temperature alone is not a sufficient measure of hardness over the entire energy range. However we find that in this case both the blackbody temperature and the power-law index independently correlate with the burst intensity. Figure 3*d* demonstrates yet another trend in spectral evolution: we see an example where the "temperature" shows a negative correlation during pulse rise and a positive correlation with burst intensity during the pulse decay phase. This illustrates the diversity in spectral evolution of bursts which belong to this subclass.

A majority of the bursts with varying pulse profiles show a good correlation of the spectral hardness with count rate (correlation coefficient ranging from 0.64 to 0.98). In cases where more than one model function was fitted, different hardness parameters of different models (like the "temperature" in eqs. [2] or [3] and the power-law index in eq. [1]) show similar or identical evolution during the burst. Hence the correlation

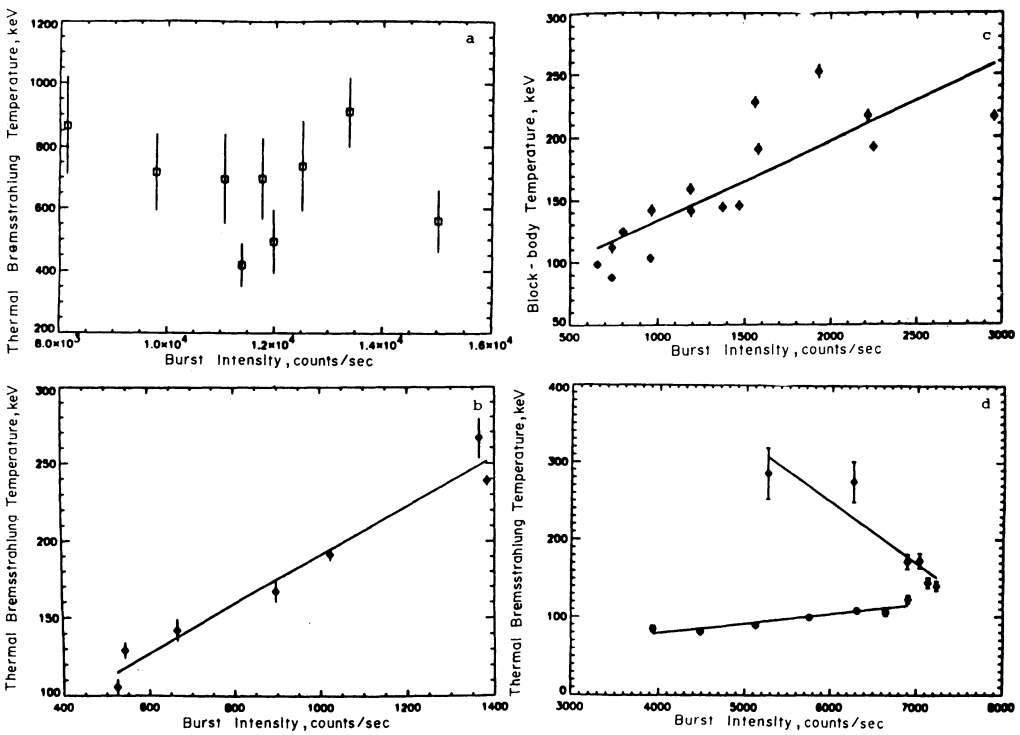

FIG. 3.—Spectral hardness parameters derived from the model fits to the segmented burst spectra are plotted against the burst intensity (background-corrected count rate) for four typical bursts. Thermal bremsstrahlung "temperatures" in keV for (*a*) 1B 910602, (*b*) 1B 910717, and (*d*) 1B 920216 and (*c*) blackbody "temperature" for 1B 910814. The spectra 1B 910814 were fitted to a sum of blackbody and power-law models for burst. In (*d*) the part of the curve wherein the "temperature" falls with increasing intensity corresponds to the rising edge of the burst profile, while the other corresponds to the falling edge.

does not depend on the spectral model chosen to fit the data. This result is also borne out by a similar analysis carried out on the data from the second brightest detector for the same burst, which also rules out possible systematic effects due to differences in the detector response functions for different burst incident angles.

If the timescale during which spectral characteristics change is shorter than the available time resolution, then one would expect a significant deviation from the conventional evolution pattern mentioned above. This could be the case in 1B 910814 (Fig. 3*c*) where we see a significant spread in the plot of "temperature" versus burst count rate. In the case of 1B 920216 (Fig. 4*d*) the integration times of the spectra are smaller than the pulse rise time. Hence we can see differences in the spectral evolution during the rise and decay phase of the burst time profile. We therefore prefer to use the hardness ratio, with a best time resolution of 64 ms, as a parameter to measure spectral hardness.

4.2. *High Time Resolution Spectral Evolution*

Figure 4 shows the time evolution of the FHPs obtained by fitting the spectra to models as described above and the hardness ratios during the course of four typical bursts. In all cases the hardness ratio evolution is consistent with the evolution of the FHPs. This shows that hardness ratio is a good parameter for the study of spectral evolution of gamma-ray bursts.

From Figure 4 it can also be seen that in each of the four cases, the variation of the FHPs show a continuous hard to soft evolution during the course of a GRB. This is a general property of a majority of the GRBs in this subset.

For burst 1B 910814, the correlation coefficient between the "blackbody temperature" and the (background-subtracted) average burst count rate is 0.82. The corresponding correlation coefficients for the hardness ratios are 0.76, 0.83, 0.81, and 0.83 at time resolutions of 64, 128, 320, and 640 ms, respectively. This shows that the correlation is valid at least down to timescales as short as 64 ms. Figures 5*a* and 5*b* show time histories of the hardness ratio (*solid line*) and the burst intensity (*dotted line*) in the time range 0–5 s and 5–10 s since trigger, respectively. The bin width is 64 ms. The remarkable similarity between the two time histories as well as the narrow features seen in the hardness ratio time profiles may indicate significant variation of spectral hardness during a time duration as short as 64 ms. A search for spectral variability during even a smaller timescale (using medium energy resolution [MER] data which has a time resolution of 16 ms) is inconclusive because the variations in hardness ratio become comparable to statistical fluctuations.

Figure 6 shows the time histories of the spectral hardness ratio and the intensity (background-corrected count rate; *dotted line*), suitably scaled, on the same plot for four typical bursts. It may be noted that for bursts which show a correlation between FHP and burst intensity for most part of the burst, the two time histories are similar in shape but shifted in time. In a majority of the cases the hardness leads the counting rate (as seen in Figs. 6*c* and 6*d*). In two cases (among 19 in this

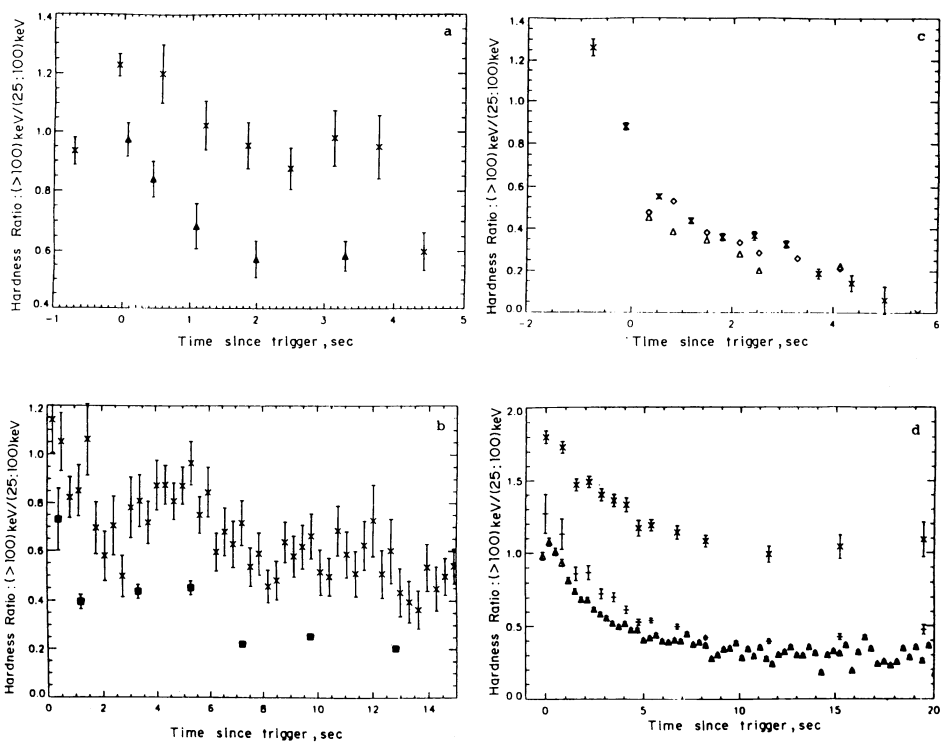

FIG. 4.—Relative variations of the various hardness parameters of the segmented spectra from four GRBs: (*a*) 1B 910629.—The crosses represent the hardness ratio (HR) with time resolution of 640 ms, and the filled triangles represent the optically thin thermal bremsstrahlung (OTTB) "temperatures" in keV (scaled down by a factor of 400). (*b*) 1B 910717.—The crosses represent HR with a time resolution of 640 ms, while diamonds represent OTTB "temperatures" (keV), and triangles represent Comptonized spectrum "temperatures" (COMP; in keV) (both scaled down by a factor of 400). (*c*) 1B 910718B.—The crosses represent HR with a time resolution of 128 ms, while filled squares represent OTTB "temperatures" in keV (scaled down by a factor of 400). (*d*) 1B 920216.—The triangles represent the hardness ratio with a resolution of 320 ms, while the crosses represent the OTTB "temperatures" (keV) (scaled down by a factor of 200), and the crosses represent parameters proportional to the power-law indices. The plotted parameter is $3.5 + \alpha$. The similarity in the evolution of all the three spectral parameters show that the spectral evolution is model independent.

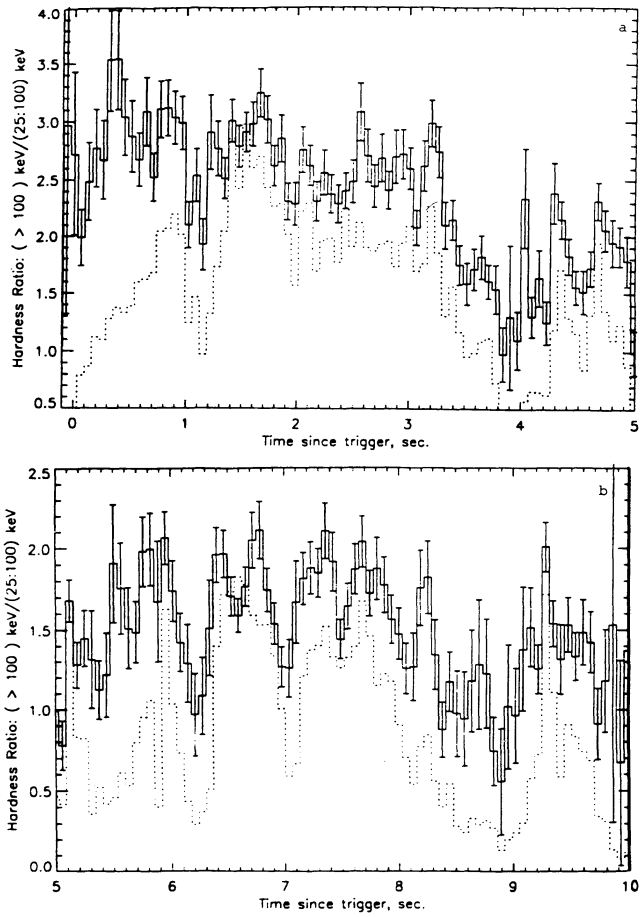

FIG. 5.—Time histories of hardness ratio (*solid histogram*) and burst intensity (*dotted histogram*) for burst 1B 910814 shown in two parts for clarity. The time resolution is 64 ms. (*a*) The first 5 s of the burst with respect to trigger time; (*b*) 5–10 s of the burst. The errors shown for hardness are only statistical. The similarity between the hardness ratio and counting rate in both cases (*a*) and (*b*) show a correlation between them. Fine structures seen in the hardness ratio time history provide evidence for the spectral variations on very short timescales (64 ms).

subset), the hardness lags (Fig. 6*b*). Except for this difference, these bursts behave similarly to most other 15 bursts showing a similarity in the time histories. In two other cases (1B 910421 and 1B 910602), the hardness ratio does not show significant variation during the entire burst as seen in Figure 6*a*.

It can be seen from Figs. 6*b* and 6*c* that the hardness ratio time profile has its own rise and decay time. The time lag between the peaks of the hardness ratio profile and the count rate profile has been estimated for those bursts which show a positive lag. This time lag, τ_l, is proportional to the rise time, τ_r, of the burst profile, and the correlation coefficient is 0.8 (Fig. 7). This relationship can be written as: $\tau_l = K \times \tau_r^{(0.9 \pm 0.2)}$, where K is a constant.

5. DISCUSSION

We studied a sample of 19 bursts using their hardness ratios as their spectral hardness parameters. For seven randomly chosen bursts, the analysis was also carried out using the conventional spectral fitting techniques in order to confirm the consistency between the two procedures. It is clear from this analysis that the GRBs which belong to this subclass do not share common spectral evolution properties. The results from the two methods establish that the spectral evolution of gamma-ray bursts does not depend significantly on the parameters chosen to represent the spectral hardness.

Gamma-ray burst continuum spectra recorded by the BATSE spectroscopy detectors were studied in detail by Band et al. (1993) and Hurley et al. (1991), who found that there is no universal spectral model that fits all the integrated burst spectra and that there is no correlation between the burst spectral parameters and the burst morphology. This is consistent with the present analysis of bursts which have similar morphology. The diverse spectral evolution seen in our subset of bursts reflects that seen in a larger sample comprising a variety of bursts, showing that bursts cannot be classified based on their pulse shapes alone. A high time resolution study of short gamma-ray bursts observed by BATSE also shows a similar diversity in spectral evolution (Bhat et al. 1993).

Previous results on the spectral evolution studies have also shown that burst continua are often hardest in the initial phase and then soften with time (Mazets et al. 1982; Teegarden 1982; Kuznetsov et al. 1986; Band et al. 1991) which is consistent with the present analysis for a majority of bursts in the subset. We find exceptions to this general behavior in two bursts which show no significant change in the spectral hardness throughout. In addition, we also find that in a majority of the cases there is a hard to soft spectral evolution within individual pulses in a burst as was reported by Norris et al. (1986). For burst 1B 910717 in particular (Fig. 4*b*), it may be noted that the energy range used for spectral fitting was 100–1500 keV. In this case also one can see a characteristic hard to soft evolution. In other words, the spectral softening is a wide-band property of GRBs and is not simply due to absorption of the continuum photons below 100 keV. This confirms the observation first made by Norris et al. (1986).

A possible correlation between the hardness "temperature" and burst intensity was first suggested by Golenetskii, Ilyinskii, & Mazets (1984), based on the *KONUS* data. Later studies of the *SIGNE* data by Kargatis et al. (1991) confirm this result and further suggest that burst luminosity computed from the observed spectra in counts space varies as T^{γ}, where T is the "temperature" in keV (being one of the parameters in the model in eqs. [2]–[4]), and γ is nominally 1.6 (but varies in the range 0.5–2.5, from burst to burst). In the present case the value of γ varies from 1.4 for 1B 910814 to 3.4 1B 910629. Such a correlation between the spectral hardness and burst intensity has been suggested to imply that the instantaneous value of the source luminosity is determined by the temperature in the emitting region (Mazets et al. 1983). However, this is a model-dependent conclusion.

One model which invokes the possibility of Compton scattering of γ-ray photons in the immediate vicinity of the GRB source is proposed by Brainerd (1993). According to the model, the observed GRB spectrum is an outcome of a power-law type source spectrum undergoing attenuation through Compton scattering in an optically thick medium. However, in order to explain the observed correlation of the spectral hardness with burst intensity, one would require the optical depth of the medium to vary with the burst intensity and photon energy. The latter constraint could explain the origin of soft lag.

The soft lag, on the other hand, could also result from a geometric constraint at the source as discussed by Katz (1994). This cosmological model considers the production of gamma rays in a GRB resulting from the interaction of relativistic

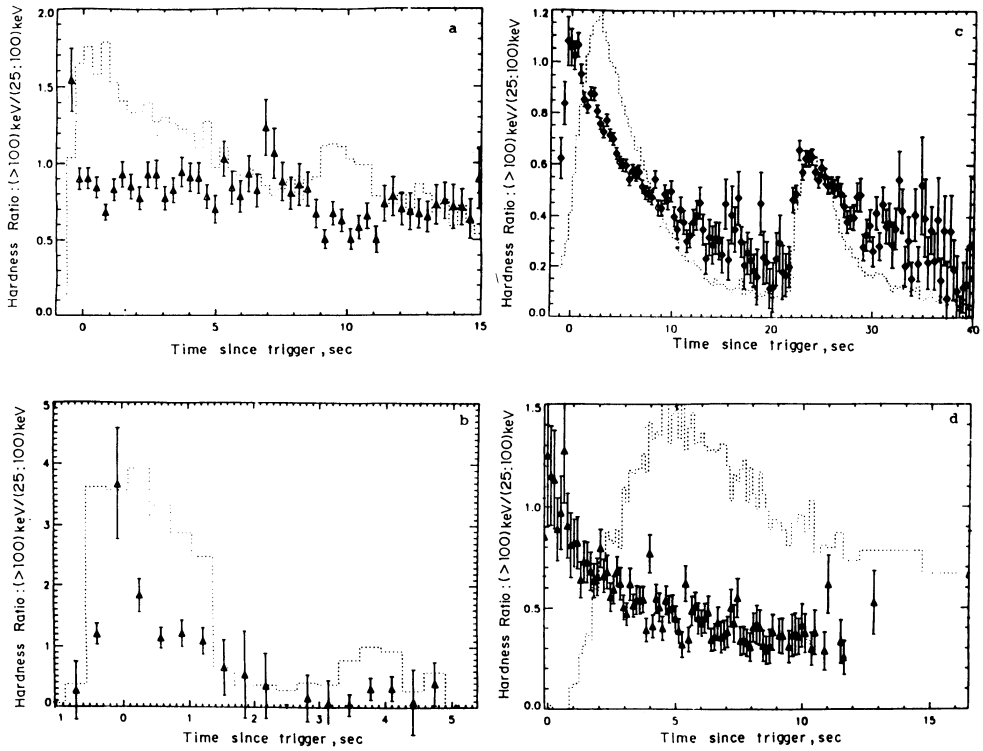

FIG. 6.—A relative comparison of the time variations of hardness ratio and burst intensity for four typical bursts. (*a*) 1B 910602, where the hardness ratio evolution is independent of the burst intensity; time resolution, 320 ms. (*b*) 1B 910714, where the hardness lags with respect to the burst intensity; time resolution, 128 ms. (*c*) 1B 911031, where two pulse profiles evolve similarly but independently. The hardness leads burst intensity in both cases. (*d*) 1B 920216.

fireball debris with the surrounding cloud. In this case the radiation produced on the expanding spherical shell at a large angle, θ, with respect to the line of sight will be softer because of Doppler shift, and it also will be delayed with respect to the harder photons which are observed at smaller values of θ. However, the delays predicted by this model on the basis of the assumed parameters are too small compared to observations.

The soft lag observed in a majority of the GRBs in this subset is not specific to these bursts. A similar behavior was reported for short gamma ray bursts by Bhat et al. (1992b) who showed that the time lag varies as log (E), where E is the mean photon energy (Bhat et al. 1992).

The fast spectral variability seen in 1B 910814 could place a limit on the size of the production region. The observation of spectral variability on the 64 ms timescale would imply that the size of the effective emission region is $\lesssim 2 \times 10^4$ km, assuming no relativistic effects. This is not inconsistent with the model which predicts an effective length scale of ~ 400 km for the region emitting the radiation (Katz 1994). The fastest spectral variability in a gamma ray burst reported previously is 0.25 s in GB 820827c observed by the *KONUS* experiment (*Venera 13* and *14*). This was limited by the instrument resolution and hence can be considered only as an upper limit (Mazets et al. 1983; Mitrofanov et al. 1984). Rapid spectral variability in 0.25 s was also detected in GB 781104 observed by the *SIGNE* experiment (*Venera 11* and *12*). Since an emission feature at 400 keV was also detected in the same burst, the authors attribute the fast spectral variability to the presence of annihilation line flashes in the burst (Barat et al. 1984).

The GRB pulse rise times (shown in Table 1) when plotted against the average hardness ratio show a rather weak evidence that the hardness ratio and rise times are inversely correlated (correlation coefficient of -0.2). This may suggest that rise time of the pulse profile is one morphological parameter that could be related to the average spectral hardness. This is consistent with the analysis by Kouveliotou et al. (1991), who found that a sample of bursts with short risetimes showed hardness ratios on average higher than other bursts.

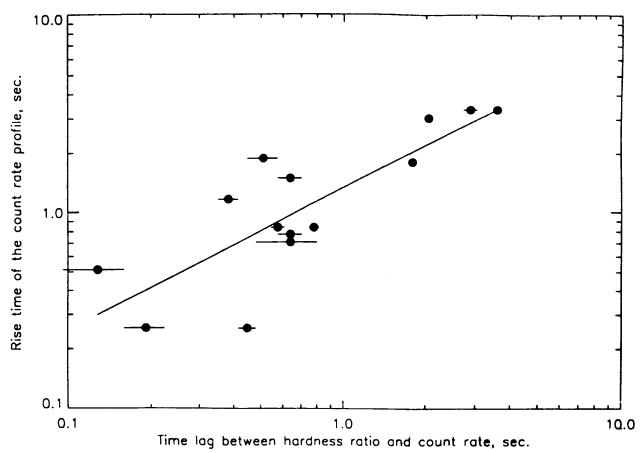

FIG. 7.—A plot of the burst rise time as a function of the time lag between the peaks of the hardness profile and the burst profile. There seems to be good correlation. The correlation coefficient is 0.8.

We thank M. S. Briggs, R. D. Preece, and J. J. Brainerd for fruitful discussions and comments on the manuscript. We also thank the members of the BATSE data operations team.

REFERENCES

Band, D., et al. 1991, in Gamma Ray Bursts, ed. W. S. Paciesas & G. J. Fishman (New York: AIP), 169
Band D., et al. 1993, ApJ, 413, 281
Barat, C., Hurley, K., Niel, M., Vedrenne, G., Mitrofanov, I., Estulin, V. I., & Zenchenko, V. M., & Dolidze, V. 1984, ApJ, 286, L11
Bhat, P. N., Fishman, G. J., Meegan, C. A., Wilson, R. B., Kouveliotou, C., Paciesas, W. S., & Pendleton, G. N. 1992a, in Compton Gamma Ray Observatory, ed. M. Friedlander, N. Gehrels, & D. J. Macomb (New York: AIP), 912
Bhat, P. N., Fishman, G. J., Meegan, C. A., Wilson, R. B., & Paciesas, W. S. 1992b, in Compton Gamma Ray Observatory, ed. M. Friedlander, N. Gehrels, & D. J. Macomb (New York: AIP), 953
———. 1993, Proc. 23d Internat. Cosmic Ray Conf. (Calgary), 1, 97
Brainerd, J. J. 1993, ApJ, 410, 507
Cline, T. L., & Desai, U. D. 1975, ApJ, 196, L43
Cline, T. L., Desai, U. D., Klebesadel, R. W., & Strong, I. B. 1973, ApJ, 185, L1
Fishman, G. J., et al. 1989, Proc. GRO Science Workshop GSFC, Greenbelt, MD, ed. W. N. Johnson, 2-39
Golenetskii, S. V., et al. 1983, Nature, 306, 451
Golenetskii, S. V., Ilyinskii, V., & Mazets, E. P. 1984, Nature, 307, 41
Hurley, K., et al. 1991, in Gamma Ray Bursts, ed. W. S. Paciesas & G. J. Fishman (New York: AIP), 195
Jourdain, E. 1990, Ph.D. thesis, C.E.S.R., Paul Sabatier University, Toulouse
Kargatis, V. E., Liang, E. P., & Hurley, K. C. 1991, in Gamma Ray Bursts, ed. W. S. Paciesas & G. J. Fishman (New York: AIP), 201
Katz, J. I. 1994, ApJ, 422, 248
Kouveliotou, C., Meegan, C. A., Fishman, G. J., Bhat, P. N., Briggs, M. S., Koshut, T. M., Paciesas, W. S., & Pendleton, G. N. 1993, ApJ, 413, L101
Kouveliotou, C., Paciesas, W. S., Fishman, G. J., Meegan, C. A., & Wilson, R. B. 1991, in Compton Observatory Science Workshop, ed. C. R. Shrader, N. Gehrels, & B. Dennis (NASA CP-3137), 61
Kuznetsov, A. V., Sunyaev, R. A., Terekhov, O. V., Barat, C., & Boer, B. 1986, Soviet Astron. Lett., 12, 315
Loredo, T. J., & Epstein, R. I. 1989, ApJ, 336, 896
Matz, S. M., Forrest, D. J., Vestrand, W. T., Chupp, E. L., & Share, G. H. 1985, ApJ, 288, L37
Mazets, E. P., Golenetskii, S. V., Guryan, Yu. A., Aptekar, R. L., & Ilyinskii, V. N. 1983, in Positron-Electron Pairs in Astrophysics, ed. M. L. Burns, A. K. Harding, & R. Ramaty (New York: AIP), 36
Mazets, E. P., Golenetskii, S. V., Ilyinskii, V. N., Guryan, Yu. A., & Aptekar, R. L. 1982, Ap&SS, 82, 261
Mitrofanov, I. G., Dolidze, V. S., Barat, C., Vedrenne, G., & Niel, M. 1984, Soviet Astron., 28, 547
Norris, J. P., Share, G. H., Messina, D. C., Dennis, B. R., & Desai, U. D. 1986, ApJ, 301, 213
Pendleton, G. N., Paciesas, W. S., Lestrade, J. P., Fishman, G. J., Wilson, R. B., & Meegan, C. A. 1989, in Proc. GRO Science Workshop GSFC, ed. W. N. Johnson, 4-547
Schaefer, B. E. 1993, ApJ, 404, L87
Schaefer, B. E., et al. 1992, in The Compton Observatory Science Workshop, ed. C. R. Schrader, N. Gehrels, & B. Dennis (NASA CP-3137), 53
Schneid, E. J., et al. 1992, A&A, 255, L13
Teegarden, B. J. 1982, in Gamma Ray Transients and Related Astrophysical Phenomena, ed. R. E. Lingenfelter, J. C. Higdon, & D. M. Worrall (New York: AIP), 352